Catalysis Letters (2018) 148:3402–3412
https://doi.org/10.1007/s10562-018-2535-9

Highly Catalytic Activity of Ba/γ-Ti–Al_2O_3 Catalyst for Aldol Condensation of Methyl Acetate with Formaldehyde

Qiang Bao[1] · Hui Qi[3] · Chunlei Zhang[2] · Chunli Ning[2] · Yi Zhang[2] · Ye Jiang[1] · Yifan Wu[1] · Wenying Gui[1] · Zhenlu Wang[1]

Received: 22 June 2018 / Accepted: 20 August 2018 / Published online: 31 August 2018

Abstract

In this work, titanium-doped mesoporous Al_2O_3 (γ-Ti–Al_2O_3) was prepared by an evaporation-induced self-assembly method and used as a carrier of Ba/γ-Ti–Al_2O_3 catalyst to catalyze the aldol condensation of methyl acetate with formaldehyde to methyl acrylate in a fixed-bed reactor. The catalysts were characterized by X-ray diffraction, X-ray photoelectron spectroscopy, N_2 adsorption–desorption, pyridine absorption performed via Fourier transform infrared spectroscope (Py-IR), and NH_3 and CO_2 temperature-programmed desorption (NH_3 and CO_2-TPD). Experimental results indicated that the doping of the titanium species into the frame work of mesoporous Al_2O_3 (γ-Ti–Al_2O_3) had a significant influence on the catalytic activity via modifying the acid–base surface properties of the catalyst. Furthermore, the Ba/γ-Ti–Al_2O_3 catalyst demonstrated excellent catalytic performance, with a methyl acetate conversion rate of 50% and methyl acrylate selectivity up to 90.2%. Compared with the Ba/Al_2O_3 catalyst, the Ba/γ-Ti–Al_2O_3 catalyst had better catalytic activity, stability and potential for practical application, which was likely due to an increased number of Lewis acid sites, especially the medium acid sites.

Graphical Abstract

Barium supported mesoporous γ-Ti–Al_2O_3 catalyst was found to be an effective catalyst for vapor phase aldol condensation of methyl acetate with formaldehyde.

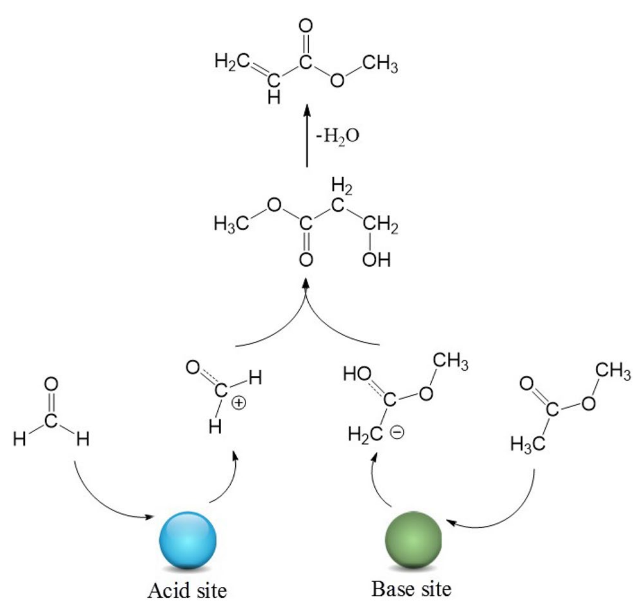

Electronic supplementary material The online version of this article (https://doi.org/10.1007/s10562-018-2535-9) contains supplementary material, which is available to authorized users.

Extended author information available on the last page of the article

Keywords γ-Al_2O_3 · Ba/γ-Ti–Al_2O_3 catalysts · Vapor-phase aldol condensation · Methyl acrylate · Lewis acid sites

1 Introduction

As fundamental industrial monomers, methyl acrylate (MA) and acrylic acid (AA) are widely used in the manufacture of paint additives, adhesives, textiles, and leather treating agents [1–4]. Currently, MA is produced through esterification of methanol (MeOH) with AA, and the synthesis of AA is completed through two-step oxidations of propylene with air [5–10]. However, propylene comes from non-sustainable sources in the petrochemical industry, and its price is greatly influenced by crude oil prices. With the ever-increasing demand for petroleum, it is becoming increasingly popular to use propylene as a feedstock. Therefore, it is highly important to develop a novel and green route for AA and MA synthesis.

In recent decades, a one-step synthesis of MA and AA via vapor-phase aldol condensation of acetic acid (Aa) or methyl acetate (Ma) with formaldehyde (FA) has been researched and developed because of its simplified reaction route and common feedstocks that can be derived readily from natural gas, coal and biomass [11, 12].

Aldol condensation plays an important role in organic synthesis for C–C bond formation, and has numerous applications in the synthesis of fine chemicals [13–16]. According to previous work, the aldol condensation reaction can be catalyzed by acid/base catalysts and can readily occur over either acid, base, or acid–base bifunctional catalysts. Ai [17–21] prepared a series of solid acid catalysts using an impregnation method and found that vanadium–titanium binary phosphates and V_2O_5–P_2O_5 binary oxide can effectively catalyze the aldol condensation of HCHO with acetic acid/methyl acetate to acrylic acid and its derivatives. Based on their work, Feng et al. [22] prepared an improved VPO catalyst and achieved an optimal conversion of methyl acetate of 84.2% (including 30–35% acetic acid and 3–12% COx). They also stated that the vanadyl phosphate entity appearing in the δ-$VOPO_4$ form functions as the active component. However, Yang et al. [23] reported that the V/P atomic ratio is an essential factor determining the catalytic performance of the aldol condensation reaction, and that the optimal ratio is 1:2. The low stability of such catalysts and the difficulty of precisely controlling the V/P atomic ratio would be principal obstacles to produce MA and AA based on acid catalysts in large quantities. More attention has been paid to basic catalysts, which often include the oxides or hydroxides of alkali or alkaline earth metals supported on porous materials, because of the easier preparation and higher catalytic activity than acidic catalysts. Yan et al. [24] designed a Cs/SBA-15 catalyst, and the yield and selectivity of MA could reach 48.4 and 95.0%, respectively. Zhu et al. [25] reported a Cs–La–Sb/SiO_2 catalyst and showed the conversion of methyl acetate (20%) as well as a small yield of methyl acrylate (8%). However, they found that the activity of the best catalyst sharply decreased as the reaction progressed due to coke deposition and the irreversible loss of the Cs species.

Alumina is one of the most important catalytic materials, which is widely used as a catalyst or carrier in the automotive and petroleum industries due to its low cost, desirable textural properties (such as high surface area, mesoporosity and stability) and its Lewis acid sites [26, 27]. In our previous work, we prepared an Al_2O_3-supported barium catalyst, which showed the conversion of methyl acetate (43.4%) as well as a selectivity of methyl acrylate (92.8%) when optimized [28]. After that, we prepared an improved Ba–La/Al_2O_3 catalyst, which showed the highest (43.5%) conversion of methyl acetate with 93.9% selectivity for methyl acrylate. Although the stability of the catalyst improved significantly due to the alkaline function of La_2O_3, the activity of the Ba–La/Al_2O_3 catalyst was not obviously increased compared with Ba/Al_2O_3 catalyst [29]. Hence, development of catalyst with higher catalytic activity for the target reaction is necessary.

Combined with previous studies, we found that the Lewis acid sites on the catalyst surface played a crucial role in the aldol condensation reaction of methyl acetate with formaldehyde. For titanium oxides, it has been reported that although they have relatively low specific surface areas, the surface Lewis acid sites of TiO_2 are multivalent and stronger than those of alumina [30]. Therefore, more surface Lewis acid sites may be obtained by complexes of aluminum and titanium, which provide certain possibilities for the catalytic activity of titanium-doped mesoporous Al_2O_3 towards the target reaction.

In this paper, titanium was doped into the frame work of mesoporous Al_2O_3 (γ-Ti–Al_2O_3) or loaded on the surface of Al_2O_3 (TiO_2/Al_2O_3). The obtained materials were used as carriers to prepare γ-Ti–Al_2O_3- and TiO_2/Al_2O_3-supported barium catalysts by the incipient wetness impregnation method for the aldol condensation of methyl acetate with formaldehyde. The catalytic performances of the catalysts were carried out in a fixed-bed microreactor. The physical–chemical properties of the catalysts were studied by N_2-adsorption, XRD and XPS. The surface acidity and basicity of the catalysts were studied by CO_2-TPD, NH_3-TPD and pyridine adsorption IR. This work also details the catalyst stability and reusability and postulates a reaction route for this aldol condensation reaction.

2 Experiment

2.1 Catalyst Preparation

Methyl acetate (≥ 99.0%), methanol (CH_3OH; ≥ 99.0%), trioxymethylene (≥ 98.0%), barium acetate ($Ba(CH_3COO)_2$; ≥ 99.0%) and D-glucose monohydrate of analytical grade were purchased from the Sinopharm Chemical Reagent Company. Aluminum isopropoxide ($C_9H_{21}AlO_3 \geq 98.0\%$) and tetrabutyl titanate ($C_{16}H_{36}O_4Ti \geq 99.0\%$) were purchased from the Aladdin Industrial Corporation. Aluminum isopropoxide [$Al(OiPr)_3$] was used as the Al source and tetrabutyl titanate (TBOT) as the Ti source. Mesoporous γ-Ti–Al_2O_3 (Al/Ti = 75) was prepared by the evaporation-induced self-assembly method [31, 32]. In a typical procedure, $Al(OiPr)_3$ (32.7 g), glucose (28.8 g) and TBOT (0.73 g) were added into 432 mL deionized water at room temperature. After stirring for 6 h, the pH of the mixture was adjusted to 5.5 by using a diluted aqueous nitric acid (10 wt%) solution. The resulting solution was continuously stirred for 24 h and then heated at 100 °C in open air to remove water and all other volatiles. The final solid was calcined at 600 °C for 6 h to obtain γ-Ti–Al_2O_3. Al_2O_3 was prepared by the above procedure in the absence of TBOT. As references, titanium oxide loaded Al_2O_3 (TiO_2/Al_2O_3) material with an Al/Ti ratio of 75 was prepared by the incipient wetness impregnation method. The Ba/γ-Ti–Al_2O_3 catalyst was prepared as follows. Typically, the support γ-Ti–Al_2O_3 (5 g) was impregnated with 7 mL of an aqueous solution containing the desired amount of $Ba(CH_3COO)_2$ (0.44 g), and the mixture was stirred for approximately 2 h at room temperature. Afterwards, water in the mixture was evaporated at a temperature of 80 °C under atmospheric pressure. The dried materials were next calcined in a muffle furnace at 600 °C for 5 h with a 5 °C/min heating ramp rate. After natural cooling, the Ba/γ-Ti–Al_2O_3 catalyst was obtained. The other supported catalysts were prepared in the same way.

2.2 Catalyst Characterization

X-ray diffraction (XRD) patterns were measured with an Empyrean X-ray diffractometer using a nickel filtered Cu Kα source with a wavelength of 0.154 nm. An accelerating voltage of 40 kV and a current of 40 mA were used. A slit width of 0.25° was used on the source. Scans were collected using a PIXcel^{3D} detector. N_2 adsorption/desorption isotherms were measured using a Micromeritics ASAP 2010N analyzer. Specific surface areas were calculated using the BET model. Pore size distributions are evaluated from desorption branches of nitrogen isotherms using the BJH model. X-ray photoelectron spectroscopy (XPS) measurements were conducted on ESCALAB250 spectrophotometer. The electron binding energies were referenced to the C 1s (Eb = 284.6 eV) peak. Temperature programmed desorption (TPD) of NH_3 and CO_2 were used to characterize the acidic and basic sites over the studied catalysts, respectively. The TPD experiments were conducted using a ChemBET Pulsar TPR/TPD instrument (Quantachrome Instruments) with a built-in TCD detector. Typically, 50 mg catalyst was used in each measurement. The catalyst was first purged with He (UHP grade, Airgas) at 600 °C for 0.5 h with a 10 °C/min heating ramp rate, then cooled to 80 °C. A flow of CO_2 (research grade, Airgas) or NH_3 (electronic grade, Airgas) was introduced into the tubular catalyst bed for 30 min at 80 °C for CO_2 or NH_3 adsorption. After purging the catalyst bed for approximately 30 min with He to evacuate the physiosorbed NH_3 or CO_2, the catalyst was heated to 600 °C with a 10 °C/min heating ramp rate. The change in thermal conductivity due to the concentration change of NH_3 or CO_2 in the effluent was recorded on TCD detector. IR spectra were recorded on a Nicolet Impact spectrometer at 4 cm^{-1} optical resolution. Prior to the measurements, 20 mg of the catalysts were pressed into self-supporting discs and activated in the IR cell attached to a vacuum line at 250 °C for 0.5 h. The adsorption of pyridine (Py) was performed at 50 °C for 30 min. The excess pyridine was further evacuated at 50 °C for 0.5 h. After elimination of the physically absorbed pyridine, the sample was cooled down to room temperature for collection of the IR spectrum; then, the sample was returned to reaction conditions and heated at a further temperature.

2.3 Catalyst Evaluation

The vapor phase aldol condensation reaction of methyl acetate with formaldehyde was conducted in a fixed-bed reactor under atmospheric pressure. Typically, 500 mg of catalyst was loaded to the center (supported by a quartz frit) of a stainless-steel tube reactor that was 30 cm long with a 0.8 cm inside diameter. The mixed solution of methyl acetate and formaldehyde was fed into the reactor using an advection pump with a typical flow rate of 0.06 mL/min. The products were identified and analyzed by gas chromatography (GC-8A, FID) on a 60 m capillary column DB-WAX.

The mixed reactant consisting of a molar ratio of 1:2:2 Ma/FA/CH_3OH, was fed to the reactor using a metering pump. FA was fed as trioxane, which was dissolved in Ma. The formation of acetic acid because of the hydrolysis of Ma causes pipeline corrosion and reacts with FA to form acrylic acid. Thus, the methanol was added to inhibit the hydrolysis of Ma into acetic acid. The catalysts were evaluated based on their catalytic performance. The definition of methyl acetate conversion and product selectivity was as follows:

$$\text{Ma Conversion (\%)} = \left(\text{Ma}_{\text{in}} - \text{Ma}_{\text{out}}\right)/\text{Ma}_{\text{in}} \times 100\%$$

$$\text{MA Selectivity (\%)} = \text{MA}/\left(\text{Ma}_{\text{in}} - \text{Ma}_{\text{out}}\right) \times 100\%$$

$$\text{MA Yield (\%)} = \text{Ma Conversion (\%)} \times \text{MA Selectivity (\%)}$$

3 Results and Discussion

3.1 Physicochemical Properties

The XRD patterns of the γ-Ti–Al_2O_3, TiO_2/Al_2O_3, Al_2O_3 and TiO_2 samples are presented in Fig. 1. From Fig. 1, we can see that typical gamma phase was generated in synthetic Al_2O_3 samples (JCPD no. 00-046-1131), designated by γ-Al_2O_3. No diffraction peaks due to Ti species were detected on TiO_2/Al_2O_3, which deduced that TiO_2 was present in a highly dispersed state on the surface of TiO_2/Al_2O_3. For TiO_2, diffraction peaks at $2\theta = 25.3°$ and 48.0° are assigned to anatase, and the peaks at $2\theta = 27.2°$, 35.9°, 41.0°, 54.1°, 56.4°, and 68.7° are attributed to rutile TiO_2. For γ-Ti–Al_2O_3 sample, the characteristic peak of γ-Al_2O_3 is retained, and a weak peak appeared at 25.3°, assigned to anatase. The XRD patterns of the Al_2O_3-, TiO_2-, TiO_2/Al_2O_3-, and γ-Ti–Al_2O_3-supported Ba catalysts are shown in Fig. S1. From Fig. S1, we can see that no diffraction peaks due to Ba species are detected, which is consistent with prior studies [28]. Therefore, this also indicates that barium species is highly dispersed on the surface of materials.

The surface area and pore size distribution of the studied catalysts were analyzed using N_2 adsorption–desorption. Figure 2 shows that all the samples were type IV with an H1-type hysteresis loop at high relative pressure, which was due to the capillary condensation of nitrogen in the pores [33]. The textural properties of all samples are summarized in Table 1. As shown in Table 1, Al_2O_3 demonstrated the highest specific surface area (S_{BET}, 357 $m^2\ g^{-1}$), while TiO_2 demonstrated a relatively low specific surface area (S_{BET}, 48 $m^2\ g^{-1}$). The addition of titanium species, via both surface impregnation (TiO_2/Al_2O_3) and body doping (γ-Ti–Al_2O_3), resulted in the reduction of the surface area of the catalysts. A similar behavior was also observed when barium acetate was impregnated on the carriers to prepare Ba-modified catalysts, where the presence of the Ba component decreases the surface area of the support materials. This can be ascribed to a blockage of the pores by the accumulated barium component. The pore diameters and pore volumes of all the investigated catalysts (except for TiO_2 and Ba/TiO_2) ranged from 5.4 to 6.0 nm and from 0.37 to 0.52 cc g^{-1}, respectively.

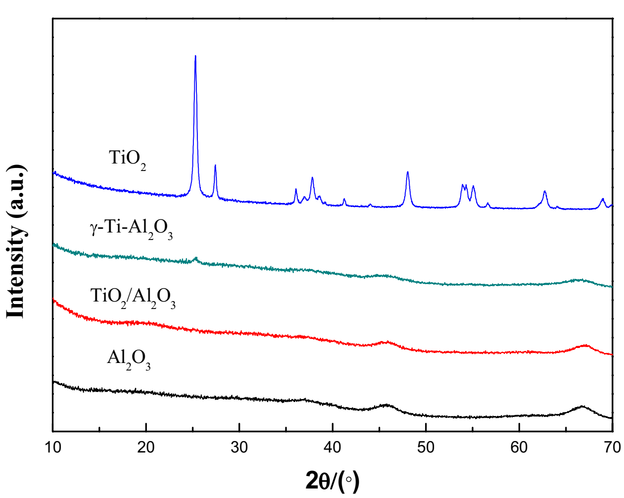

Fig. 1 The XRD patterns of the studied catalysts

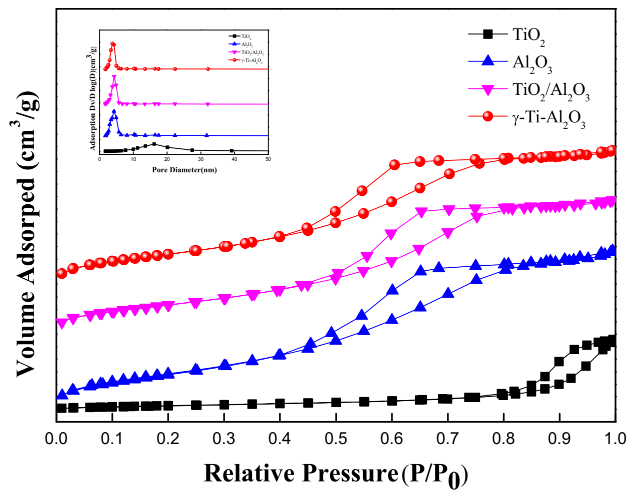

Fig. 2 N_2 adsorption–desorption isotherms and pore-size distribution of studied catalysts

Table 1 Textural properties of the supports and Ba-modified catalysts

Catalysts	S_{BET} ($m^2\ g^{-1}$)	Pore volume (cc g^{-1})	Mean pore diameter (nm)
TiO_2	48	0.19	15.5
Al_2O_3	357	0.52	5.6
TiO_2/Al_2O_3	281	0.44	6.0
γ-Ti–Al_2O_3	320	0.45	5.5
Ba/TiO_2	45	0.18	15.4
Ba/Al_2O_3	319	0.45	5.4
Ba–TiO_2/Al_2O_3	247	0.37	5.7
Ba/γ-Ti–Al_2O_3	310	0.46	5.7

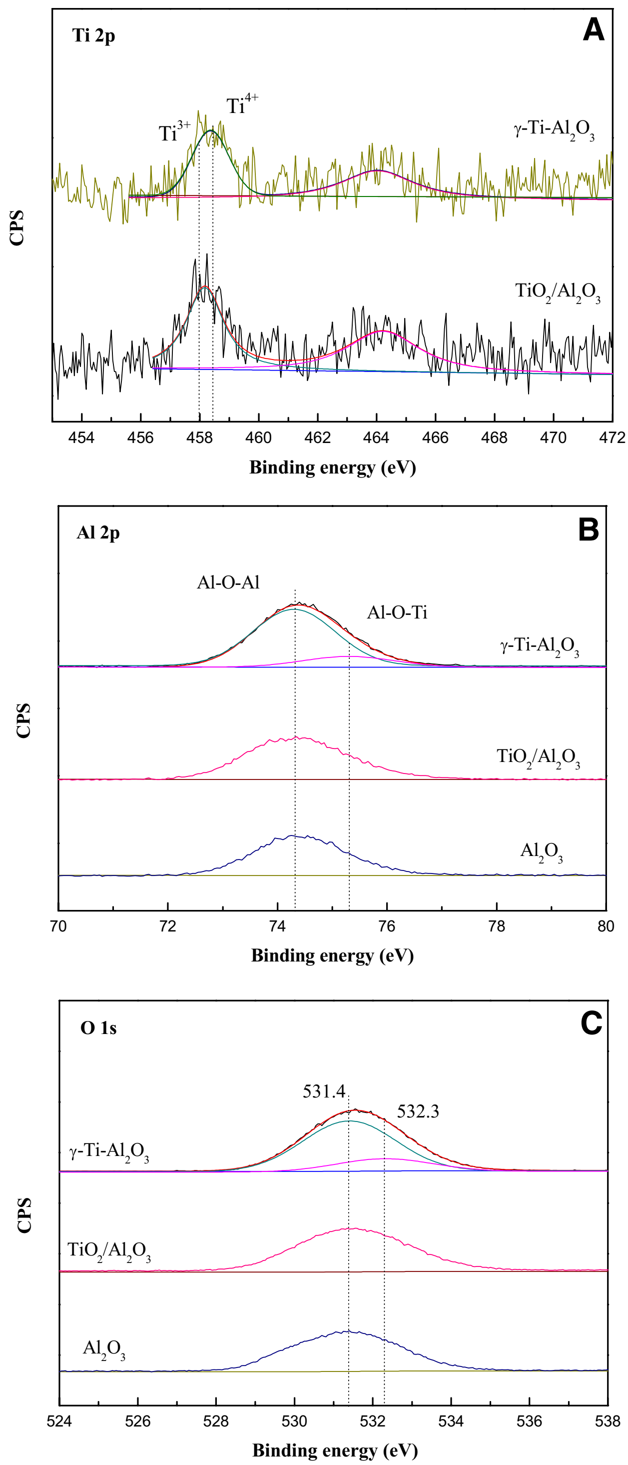

Fig. 3 Ti 2p (**a**), Al 2p (**b**) and O1s (**c**) XPS spectra of γ-Ti–Al_2O_3, TiO_2/Al_2O_3 and Al_2O_3

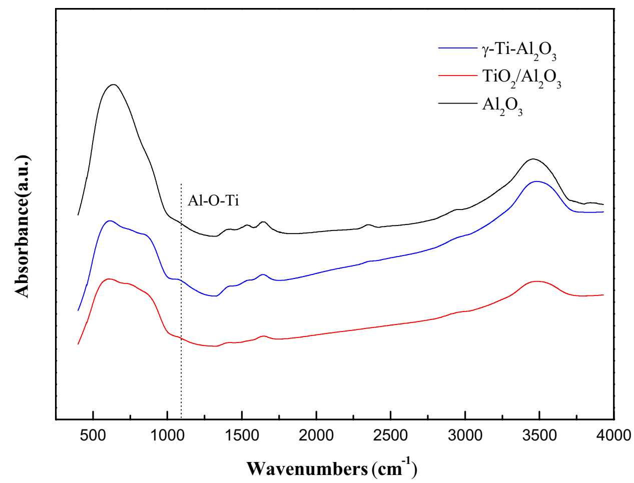

Fig. 4 FTIR spectra of γ-Ti–Al_2O_3, TiO_2/Al_2O_3 and Al_2O_3

To explore the existence of titanium species, XPS measurements of the γ-Ti–Al_2O_3, TiO_2/Al_2O_3 and Al_2O_3 were performed. Figure 3 shows the Ti 2p, Al 2p and O1s XPS spectra of different samples. According to previous research, the Ti 2p 3/2 XPS spectra could exhibit two binding energies (BEs) of Ti^{4+} at 458.9 eV and Ti^{3+} at 457.9 eV [31]. Thus, in the TiO_2/Al_2O_3 catalyst, titanium mainly existed in the form of Ti^{3+} on the surface of the material, while in the γ-Ti–Al_2O_3, titanium existed in the form of Ti^{4+}. Both Al_2O_3 and TiO_2/Al_2O_3 have similar Al 2p XPS spectra, with the binding energy (BE) of Al^{3+} at 74.3 eV, assigned to Al–O–Al [34]. In the γ-Ti–Al_2O_3 sample, however, the Al 2p XPS spectra exhibit two BEs of Al^{3+} at 74.3 and 75.3 eV, assigned to Al–O–Al and Al–O–Ti respectively [35, 36]. In addition, the peak at 1128.3 cm^{-1} appeared in the FTIR spectrum of γ-Ti–Al_2O_3, assigned to the surface Al–O–Ti groups (Fig. 4) [37], verifying titanium in the form of Al–O–Ti in the framework of γ-Ti–Al_2O_3. The O 1s XPS spectra of Al_2O_3 and TiO_2/Al_2O_3 exhibited a common peak at 531.4 eV, which is usually assigned to the lattice oxygen. In the γ-Ti–Al_2O_3 sample, besides the peak at 531.4 eV, a peak at 532.3 eV appeared, which is attributed to the chemical adsorption of oxygen at oxygen vacancies [38, 39].

3.2 Acid–Base Properties

The acid–base properties of the studied catalysts were characterized by TPD of NH_3–CO_2, shown in Figs. 5 and 6. Table 2 lists the total CO_2 and NH_3 uptakes on the basis of catalyst weight and the corresponding concentrations for the different types of acid/base sites. As shown in Fig. 5, all NH_3-TPD profiles were integrated (deconvoluted) in four fixed temperature ranges (100–180 °C, 180–230 °C, 230–300 °C, 300–500 °C) by a Gaussian peak fitting method in order to compare acidic sites of the same strength. The total NH_3 uptakes for TiO_2, Al_2O_3, TiO_2/Al_2O_3 and γ-Ti–Al_2O_3 are 40.3, 91.1, 93.2 and 114.4 mmol g^{-1} cat., respectively. The NH_3 uptakes at the four different temperature ranges for TiO_2 are 5.7, 10.2, 9.4 and 15.0 mmol g^{-1} catalyst. For Al_2O_3, the NH_3 uptakes are 14.2, 29.5, 10.2 and

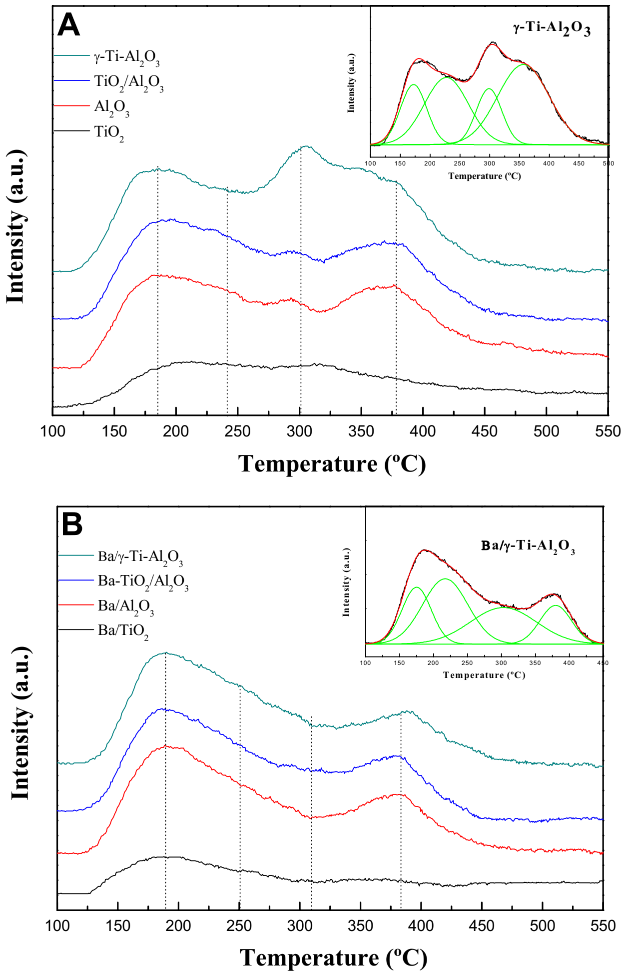

Fig. 5 NH_3-TPD patterns of the supports (**a**) and Ba-modified catalysts (**b**)

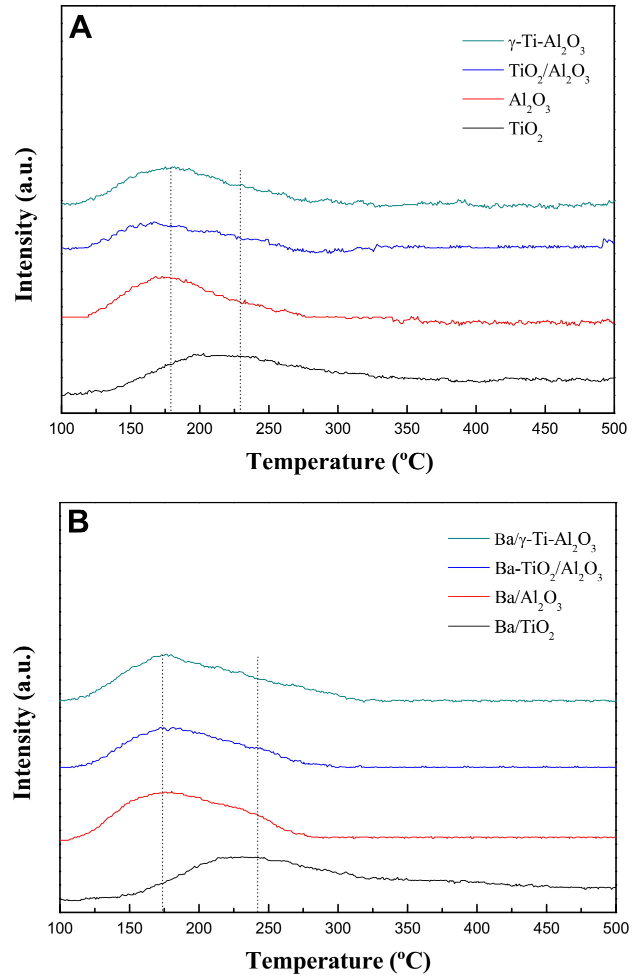

Fig. 6 CO_2-TPD patterns of the supports (**a**) and Ba-modified catalysts (**b**)

37.2 mmol g^{-1} catalyst. For TiO_2/Al_2O_3, the NH_3 uptakes are 15.7, 32.3, 10.6 and 34.6 mmol g^{-1} catalyst; whereas these are 17.8, 33.5, 16.3 and 46.8 mmol g^{-1} catalyst for γ-Ti–Al_2O_3. Overall, TiO_2 showed the least amount of acid, Al_2O_3 showed a moderate acid content, and the γ-Ti–Al_2O_3 catalyst had the most acid content. It is clearly revealed that the doping of the titanium species into the frame work of mesoporous Al_2O_3 can increase the total amount of acid centers, especially medium acid centers (in the range of 180–300 °C) and strong acid centers (in the range of 300–500 °C). The increment in strong acidity may be due to the formation of bridged hetero metal–oxygen bonds (e.g., Al–O–Ti bonds) resulting in excessive charges [31]. Compared with the catalyst carriers, the Ba-modified catalysts had a dramatically decreased NH_3 uptake at a temperature of 300–500 °C (e.g., 46.8 mmol g^{-1} cat. for bare γ-Ti–Al_2O_3 and 16.5 mmol g^{-1} cat. for Ba/γ-Ti–Al_2O_3), indicating that a large number of strong acid sites were reduced when BaO was supported on the carriers. More interestingly, the NH_3 uptake at a temperature of 180–300 °C for Ba-modified catalysts increased significantly, indicating that adding a certain amount of barium could increase the number of medium acid sites of the catalyst. This increase might be the result of an interaction between barium species and acid sites on the catalyst surface, leading to an increase in medium acid sites and a decrease in strong acid sites. Figure 6 shows the desorption profiles of CO_2 from the carriers and metal-modified catalysts. In Fig. 6, all catalysts exhibited a prominent CO_2 desorption peak in the range of 100–350 °C and the basic sites on these catalysts were arbitrarily considered weak. However, it should be noted that the maximal temperature of the desorption peak for TiO_2 is higher than that of other carrier materials, indicating a higher intensity of basic sites on the surface of TiO_2. For metal-modified catalysts, adding barium species markedly increased the total CO_2 uptake (e.g., 9.5 mmol g^{-1} cat. for bare γ-Ti–Al_2O_3 and 16.2 mmol g^{-1} cat. for Ba/γ-Ti–Al_2O_3), indicating some new base sites formed on the catalyst surface.

Table 2 List of the total CO_2 and NH_3 uptakes on the catalysts surface and the corresponding concentrations for the different types of acid/base sites

Catalyst	TiO_2	Al_2O_3	TiO_2/Al_2O_3	γ-Ti–Al_2O_3	Ba/TiO_2	Ba/Al_2O_3	Ba–TiO_2/Al_2O_3	Ba/γ-Ti–Al_2O_3
Total (mmol NH_3/g cat.)	40.3	91.1	93.2	114.4	20.2	77.9	75.2	87.6
T_1 (100–180 °C)	5.7	14.2	15.7	17.8	1.8	15.0	14.9	15.8
T_2 (180–230 °C)	10.2	29.5	32.3	33.5	6.9	24.7	24.3	33.2
T_3 (230–300 °C)	9.4	10.2	10.6	16.3	8.3	21.1	20.6	22.1
T_4 (300–500 °C)	15.0	37.2	34.6	46.8	3.2	17.1	15.4	16.5
Total (mmol CO_2/g cat.)	13.0	6.5	9.1	9.5	21.7	12.8	15.8	16.2
T (100–350 °C)	13.0	6.5	9.1	9.5	21.7	12.8	15.8	16.2

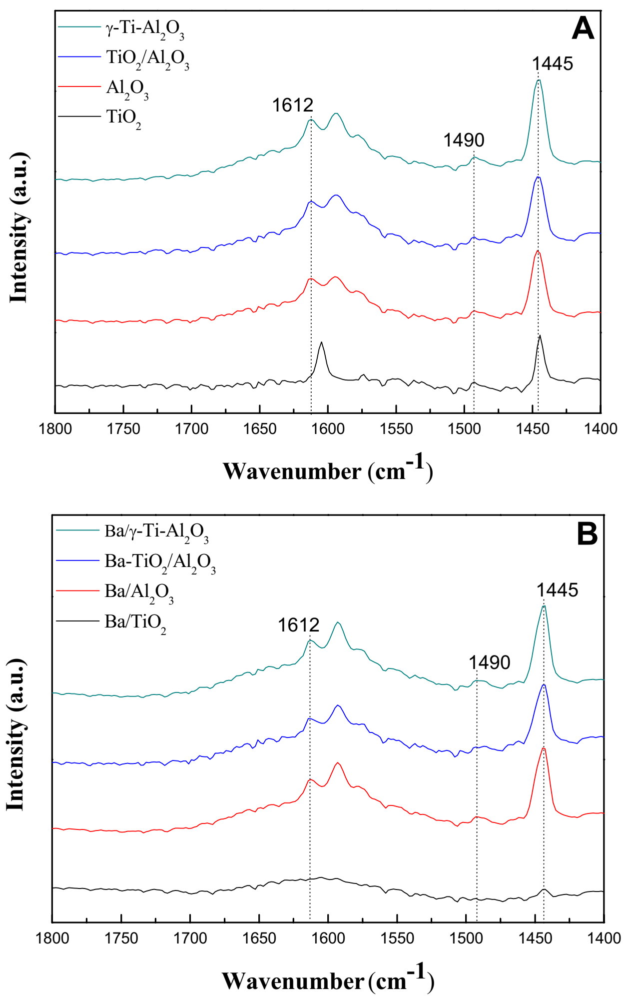

Fig. 7 FTIR spectra of pyridine adsorbed on supports (**a**) and Ba-modified catalysts (**b**) after degassing at 50 °C

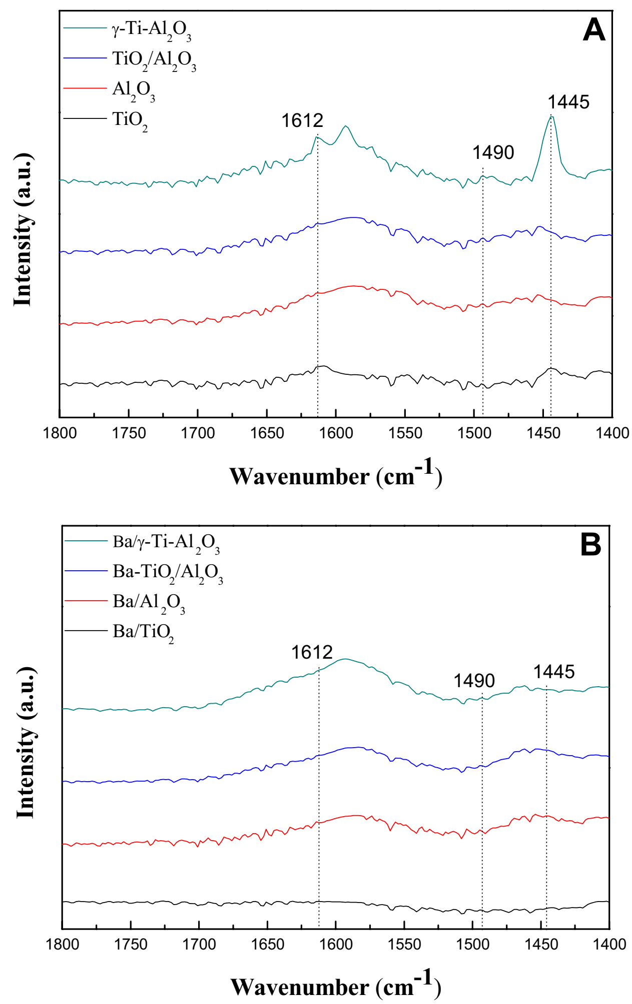

Fig. 8 FTIR spectra of pyridine adsorbed on supports (**a**) and Ba-modified catalysts (**b**) after degassing at 250 °C

As is known, pyridine can be used as a molecular probe for the determination of Lewis and Brønsted acid sites of the catalysts by monitoring the IR absorption peaks in the range of 1400–1800 cm^{-1}. To determine the nature of the acidic sites, the acid properties of the carriers and metal-modified catalysts were further characterized by FTIR spectra of pyridine adsorption. The IR results are presented in Figs. 7 and 8. In Fig. 7, all oxide materials exhibited the pyridine adsorption at 1445, 1490 and 1612 cm^{-1}. Among these, the observed IR bands at 1445 and 1612 cm^{-1} correspond to different modes of vibration of pyridine coordinated to the

Lewis acid sites. The band at 1545 cm^{-1} has been assigned to the pyridine in Brønsted acid sites (not detected in figures). The band at 1490 cm^{-1} is characteristic of the Lewis–Brønsted acid complex. On these samples, only Lewis acid sites were identified, although the Brønsted acid site was observed in a former report [40]. When pyridine desorption occurred at a relatively high temperatures (250 °C, In Fig. 8), the peaks obviously decreased, suggesting that a large amount of pyridine was removed from Lewis acid sites, which is attributed to the presence of a weakly interacting pyridine species. However, compared with other carrier materials, γ-Ti–Al_2O_3 has more obvious pyridine absorption peaks, indicating that the catalyst surface has more relatively strong Lewis acid sites. This finding is exactly consistent with the characterization results of NH_3-TPD. These results suggest that the doped titanium in the framework of Al_2O_3 altered the surface acidity of the alumina surface, particularly increasing the medium Lewis acid sites.

3.3 Activity Tests

The aldol condensation of methyl acetate with formaldehyde catalyzed by TiO_2, Al_2O_3, TiO_2/Al_2O_3, γ-Ti–Al_2O_3 and Ba-modified catalysts was carried out at 390 °C in a fixed-bed reactor. In this work, methyl acrylate was detected as the main product. Acrylic acid and acetic acid were detected as byproducts. The conversion of methyl acetate and the selectivities of acetic acid, acrylic acid and methyl acrylate based on methyl acetate were taken as the parameters to evaluate the catalytic performances.

The evaluation results of the carrier materials are depicted in Fig. 9. From Fig. 9, all the catalysts showed a certain catalytic activity towards the aldol condensation of methyl acetate with formaldehyde. For TiO_2, the initial conversion of methyl acetate was only 16.8% and the selectivity of methyl acrylate was 61.9%, which is the worst catalytic activity compared with other carrier materials. Al_2O_3 and TiO_2/Al_2O_3 catalysts showed similar activity in methyl acetate conversion, but different product distributions were observed. However, the highest yield in MA (33.2%) was obtained over the γ-Ti–Al_2O_3 sample, corresponding to an Ma conversion of 51.5% and an MA selectivity of 64.5%. BET analysis showed that the surface area order of the carrier materials was as follows: Al_2O_3 > γ-Ti–Al_2O_3 > TiO_2/Al_2O_3 > TiO_2. IR results of pyridine adsorption revealed that only Lewis acid sites were found on the surface of carrier catalysts. From the NH_3-TPD analysis, it was clear that TiO_2 gave the least amount of acid, Al_2O_3 and TiO_2/Al_2O_3 showed moderate acid content, and γ-Ti–Al_2O_3 catalyst had the most acid content. Combining the catalytic activity and selectivity with the results of characterization, we can draw the following conclusions:

1. The reason for the worst catalytic activity of TiO_2 catalyst is the low acid content and low specific surface area of titanium dioxide.
2. Al_2O_3 and TiO_2/Al_2O_3 showed similar activity in aldol condensation of methyl acetate with formaldehyde, which is largely because the catalysts have a similar amount of acidity and basicity on their surfaces.
3. The doping of the titanium species into the frame work of mesoporous Al_2O_3 (γ-Ti–Al_2O_3) had significant influence on the acidic properties of the catalyst, increasing the total amount of acid centers (especially medium acid centers and strong acid centers), which leads to the obvious increase of catalyst activity.

In our previous work, doping of alumina with BaO could be an efficient way to improve the catalytic activity and stability [28]. Therefore, a series of Ba-modified catalysts were prepared by the incipient wetness impregnation method for the aldol condensation of methyl acetate with formaldehyde to methyl acrylate. The evaluation results of the related catalysts are depicted in Fig. 10. From Fig. 10, with the addition of barium species to the supports, all the catalysts showed a slight decrease in catalytic activity to methyl acetate. However, the selectivity for methyl acrylate was significantly increased. The catalytic performances order of Ba-modified catalysts was as follows: Ba/γ-Ti–Al_2O_3 > Ba–TiO_2/Al_2O_3 ≈ Ba/Al_2O_3 > Ba/TiO_2. Among them, the Ba/γ-Ti–Al_2O_3 catalyst demonstrated the highest catalytic activity, where the initial conversion to Ma reached 50.0% and the selectivity to MA reached 90.2%. From the XRD analysis, it was clear that the barium species is highly dispersed on the surface of γ-Ti–Al_2O_3. IR results of pyridine adsorption revealed that only Lewis acid sites were found on the surface of Ba/γ-Ti–Al_2O_3, and the

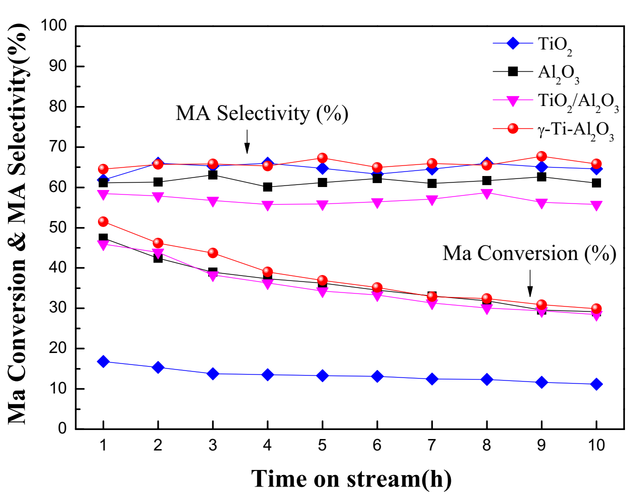

Fig. 9 The conversion of Ma and the selectivity to MA on the carrier materials

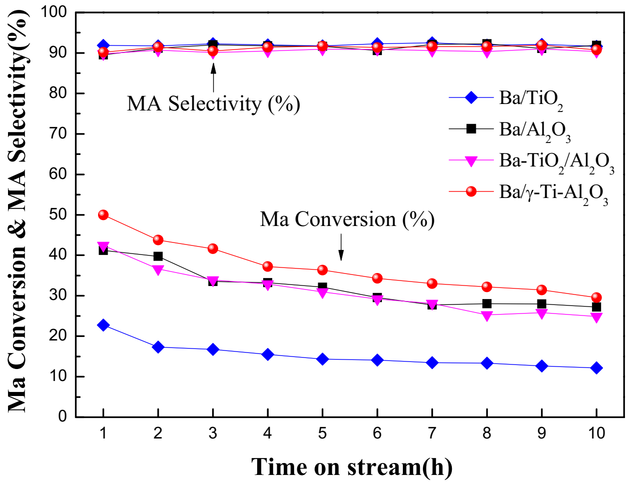

Fig. 10 The conversion of Ma and the selectivity to MA on the Ba-modified catalysts

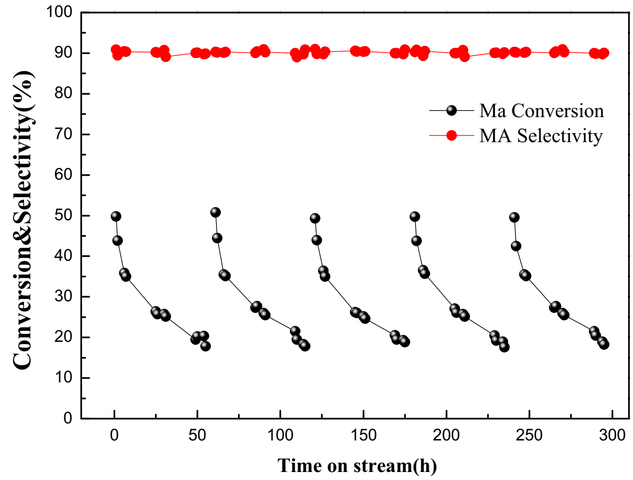

Fig. 11 The conversion of Ma and the selectivity to MA on the Ba/γ-Ti–Al_2O_3 catalyst

addition of barium species obviously reduced the number of Lewis acid sites. The TPD analysis of NH_3–CO_2 showed that the addition of barium species modified the acid–base surface properties of γ-Ti–Al_2O_3, leading to an obvious increase in medium acid sites and a decrease in strong acid sites, while providing more weak basic sites for the Ba/γ-Ti–Al_2O_3 catalysts. The dramatic change in the acid–base surface properties may be the main reason for the good catalytic activity of the Ba/γ-Ti–Al_2O_3.

Combined with the catalytic performances with the characterization results, we can conclude that the Ba/γ-Ti–Al_2O_3 catalyst had the highest catalytic activity compared with other Ba-modified catalysts, which was likely due to more Lewis acid sites on the surface of Ba/γ-Ti–Al_2O_3 catalyst, especially the medium Lewis acid sites.

3.4 Catalyst Stability and Reusability

The stability and regeneration of the Ba/γ-Ti–Al_2O_3 catalyst were also investigated at 390 °C for approximately 300 h, and the results are shown in Fig. 11. The used catalyst was regenerated by calcining in a stream of air at 500 °C for 5 h and studied under the same conditions. From Fig. 11, we can see that Ma conversion declined by nearly 70% after reaction at 60 h. In fact, the catalyst turned brown and black after the reaction. According to the previous research [41, 42], the deactivation of catalyst can be due to the formation of carbon deposition on the surface of the catalyst. Although the activity (based on the conversation of Ma) decreased gradually with reaction time as the result of the formation of carbonaceous deposits, the regenerated catalyst, after removal of carbonaceous deposits at high temperatures in a stream of air, showed nearly the same initial catalytic activity as the fresh catalyst. This result indicated that the effective components of the regenerated catalyst were not destroyed in the process of regeneration, and the activity of the Ba/γ-Ti–Al_2O_3 catalyst was relatively stable after a total reaction time of 300 h.

A probable reaction route is proposed for the vapor phase aldol condensation over the Ba/γ-Ti–Al_2O_3 catalyst in Fig. 12. First, the base sites attacked the carboxyl group of methyl acetate absorbed on the catalyst surface to form a carbanion. Next, the acid sites attacked the carbonyl group of the adsorbed formaldehyde, increasing the electrophilicity of the carbon atom. Then, the activated methyl acetate and formaldehyde reacted to form an intermediate, probably

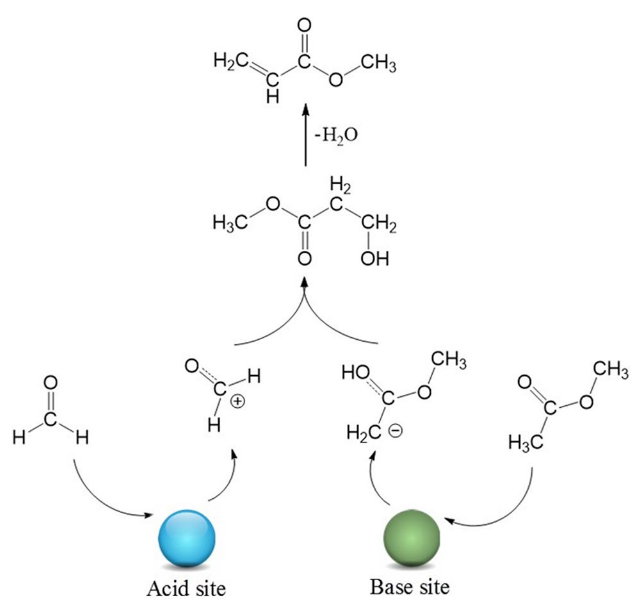

Fig. 12 Reaction mechanism for the vapor phase aldol condensation of Ma with FA over the Ba/γ-Ti–Al_2O_3 catalyst

$HOCH_2CH_2COOCH_3$, by the formation of a C–C bond. Finally, the adjacent acid sites catalyzed the rapid dehydration of the intermediate to form methyl acrylate.

4 Conclusions

Mesoporous γ-Ti–Al_2O_3 was successfully prepared by an evaporation-induced self-assembly method and used as a carrier of Ba/γ-Ti–Al_2O_3 catalyst to catalyze the aldol condensation of methyl acetate with formaldehyde to methyl acrylate in a fixed-bed reactor. The physicochemical properties of the catalysts were surveyed by XRD, N_2 adsorption–desorption and XPS. The acid–base properties of the catalysts were characterized by TPD of NH_3–CO_2 and FTIR spectra of pyridine adsorption. The characterization results showed that titanium was successfully incorporated into the framework of γ-Al_2O_3. In addition, the doping of the titanium species had a significant influence on the acidic properties of the catalyst, increasing the total amount of acid centers (especially medium acid centers and strong acid centers), which was attributed to the formation of Al–O–Ti linkages in the framework of γ-Ti–Al_2O_3. Then, the γ-Ti–Al_2O_3 was used as a carrier to prepare a Ba/γ-Ti–Al_2O_3 catalyst by the incipient wetness impregnation method to catalyze the target reaction. The experimental results showed that the Ba/γ-Ti–Al_2O_3 catalyst exhibited the best catalytic activity and selectivity on the aldol condensation of methyl acetate with formaldehyde, and the conversion of Ma achieved 50.0% with a selectivity of Ma of 90.2%, which was likely due to the more Lewis acid sites on the surface of Ba/γ-Ti–Al_2O_3 catalyst, especially the medium Lewis acid sites. After a total reaction time of 300 h, the activity of the Ba/γ-Ti–Al_2O_3 catalyst still retained its initial activity after regeneration, indicating a good reusability. Compared with the Ba/Al_2O_3 catalyst, the Ba/γ-Ti–Al_2O_3 catalyst had better catalytic activity, stability and potential for practical application.

Acknowledgements This work was supported by the technology institute of Shanghai Huayi (Group) Company and Jilin Province Science and Technology research plan (key scientific research project). (No. 20150204020GX).

Compliance with Ethical Standards

Conflict of interest There are no conflicts to declare.

References

1. Danner H, Dürms M, Gartner M, Braun R (1998) Appl Biochem Biotechnol 70:887
2. Xu X, Lin J, Cen P (2006) Chin J Chem Eng 14:419–427
3. Nagai K (2001) Appl Catal A 221:367–377
4. Vlcˇek P, Lochmann L (1999) Prog Polym Sci 24:793–873
5. Lin MM (2001) Appl Catal A 207:1–16
6. Balcells E, Borgmeier F, Grißtede I, Lintz HG, Rosowski F (2004) Appl Catal A 266:211–221
7. Ishikawa S, Yi X, Murayama T, Ueda W (2014) Catal Today 238:35–40
8. Hävecker M, Wrabetz S, Kröhnert J, Csepei L, d'Alnoncourt R, Kolen'ko Y, Girgsdies F, Schlögl R, Trunschke A (2012) J Catal 285:48–60
9. d'Alnoncourt R, Csepei L, Hävecker M, Girgsdies F, Schustera M, Schlögl R, Trunschke A (2014) J Catal 311:369–385
10. Zhai Z, Getsoian A, Bell A (2013) J Catal 308:25–36
11. Cheung P, Bhan A, Sunley GJ, Law DJ, Iglesia E (2007) J Catal 245:110–123
12. Liu J, Xue H, Huang X, Wu P, Huang S, Liu S, Shen W (2010) Chin J Catal 31:729–738
13. Trost BM, Brindle CS (2010) Chem Soc Rev 39:1600–1632
14. Palomo C, Oiarbide M, García JM (2004) Chem Soc Rev 33:65–75
15. Bui TV, Sooknoi T, Resasco DE (2017) ChemSusChem 10:1631 – 1639
16. Fäseke VC, Sparr C (2016) Angew Chem Int Ed 55:7261 – 7264
17. Ai M (1987) J Catal 107:201–208
18. Ai M (1988) J Catal 112:194–200
19. Ai M (1989) Appl Catal 48:51–61
20. Ai M (1989) Appl Catal 54:29–36
21. Ai M (1990) Appl Catal 59:227–235
22. Feng X, Sun B, Yao Y, Su Q, Ji W, Au CT (2014) J Catal 314:132
23. Yang D, Li D, Yao H, Zhang G, Jiao T, Li Z, Li C, Zhang S (2015) Ind Eng Chem Res 54:6865–6873
24. Yan J, Zhang C, Ning C, Tang Y, Zhang Y, Chen L, Gao S, Wang Z, Zhang W (2015) J Ind Eng Chem 25:344
25. Wang Y, Lang X, Zhao G, Chen H, Fan Y, Yu L, Ma X, Zhu Z (2015) RSC Adv 5:32826
26. Roy S, Mpourmpakis G, Hong DY, Vlachos DG, Bhan A, Gorte RJ (2012) ACS Catal 2:1846–1853
27. Trueba M, Trasatti SP (2005) Eur J Inorg Chem 2005:3393–3403
28. Bao Q, Bu T, Yan J, Zhang C, Ning C, Zhang Y, Hao M, Zhang W, Wang Z (2017) Catal Lett 147:1540–1550
29. Bao Q, Zhu W, Yan J, Zhang C, Ning C, Zhang Y, Hao M, Wang Z (2017) RSC Adv 7:52304
30. Jiang F, Zeng L, Li S, Liu G, Wang S, Gong J (2015) ACS Catal 5:438–447
31. Xu B, Xiao T, Yan Z, Sun X, Sloan J, González-Cortés SL, Alshahrani F, Green MLH (2006) Microporous Mesoporous Mater 91:293–295
32. Bing J, Hu C, Zhang L (2017) Appl Catal B 202:118–126
33. Bang Y, Park S, Han SJ, Yoo J, Song JH, Choi JH, Kang KH, Song IK (2016) Appl Catal B 180:179–188
34. Parlett CMA, Durndell LJ, Machado A, Cibin G, Bruce DW, Hondow NS, Wilson K, Lee AF (2014) Catal Today 229:46–55
35. Kim LH, Kim K, Park S, Jeong YJ, Kim H, Chung DS, Kim SH, Park CE (2014) ACS Appl Mater Interface 6:6731–6738
36. Zhao D, Chen C, Wang Y, Ma W, Zhao J, Rajh T, Zang L (2008) Environ Sci Technol 42:308–314
37. Gun'ko V, Zarko V, Turov V, Leboda R, Chibowski E, Pakhlov E, Goncharuk E, Marciniak M, Voronin E, Chuiko A (1999) J Colloid Interface Sci 220:302–323
38. Karthikeyan S, Dionysiou DD, Lee AF, Suvitha S, Maharaja P, Wilson K, Sekaran G (2016) Catal Sci Technol 6:530–544
39. Zhao W, Tang Y, Wan Y, Li L, Yao S, Li X, Gu J, Li Y, Shi J (2014) J Hazard Mater 278:350–359
40. Haneda M, Kintaichi Y, Hamada H (2001) Appl Catal B 31:251
41. Zhang G, Zhang H, Yang D, Li C, Peng Z, Zhang S (2016) Catal Sci Technol 6:6417
42. Ma Z, Ma X, Liu H, He Y, Zhu W, Guo X, Liu Z (2017) Chem Commun 53:9071

Affiliations

Qiang Bao[1] · Hui Qi[3] · Chunlei Zhang[2] · Chunli Ning[2] · Yi Zhang[2] · Ye Jiang[1] · Yifan Wu[1] · Wenying Gui[1] · Zhenlu Wang[1]

✉ Zhenlu Wang
wzl@jlu.edu.cn

[1] Key Laboratory of Surface and Interface Chemistry of Jilin Province, College of Chemistry, Jilin University, Qianjin Road 2699, Changchun 130012, People's Republic of China

[2] Shanghai Huayi (Group) Company Technology Research Institute, Longwu Road 4600, Shanghai 200241, People's Republic of China

[3] The Second Hospital of Jilin University, Changchun 130041, People's Republic of China